One-dimensional t-J model from a variational viewpoint

Hisatoshi Yokoyama*
Department of Physics, Tohoku University, Aramaki Aoba, Aoba-ku, Sendai 980-77, Japan

Masao Ogata†
Institute of Physics, College of Arts and Sciences, University of Tokyo, Komaba, Meguro-ku, Tokyo 153, Japan
(Received 28 June 1995; revised manuscript received 27 September 1995)

The one-dimensional (1D) t-J model is investigated by using a Gutzwiller-Jastrow-type variation method and the exact diagonalization of small systems. Variational expectation values are estimated by the variational Monte Carlo method with sufficient accuracy. First, we give detailed descriptions of the preceding paper [Phys. Rev. Lett. **67**, 3610 (1991)], where we discussed the properties of the Fermi-liquid-type Jastrow wave function as well as the Gutzwiller wave function. Secondly, these wave functions are compared with the Tomonaga-Luttinger-liquid-type wave function proposed by Hellberg and Mele. It is found that the correlation factors in short distances control bulk quantities like energy and the magnitude of the correlation functions, while the long-range part of the correlation factors determines the critical behavior of correlation functions. Finally, using these functions, charge, spin susceptibilities, and magnetization curve are estimated, which agree with the exact results. It is shown that the Mott transition in the 1D t-J model is quite different from the Brinkman-Rice transition.

I. INTRODUCTION

The t-J model is an important model to study highly correlated electron systems for its simplicity and close relationship to high-temperature superconductivity.[1] Many properties in one-dimensional (1D) systems have been clarified extensively by a number of methods: Bethe-ansatz solutions, g-ology, Tomonaga-Luttinger- (TL-) liquid theory, quantum Monte Carlo simulations, exact diagonalization studies of small clusters, and conformal field theory. We expect that the study of 1D systems will shed light on more realistic higher-dimensional systems and that comparison of the various methods with the well-established 1D results will enable us to judge the validity of such methods and approximations.

In contrast to the 1D Hubbard model,[2] the Bethe-ansatz solution does not exist in the 1D t-J model except for $J/t=0$ (spinless-fermion case) and $J/t=2$ (supersymmetric case).[3,4] In both soluble cases, a TL liquid[5] is realized and the exponents of long-range behaviors of correlation functions were calculated exactly by combining the Bethe-ansatz equations and the conformal field theory.[6–9] Also obtained were bulk quantities like spin susceptibility χ_s, charge susceptibility χ_c, specific heat coefficient, and effective transport mass, which characterize metal-insulator (Mott) transitions.[10] On the other hand, for general values of J/t, Ogata *et al.*[11] studied the low-lying energy spectrum of finite systems to obtain the correlation exponents. In the phase diagram of J/t and the electron density n [$n=N/N_a$, N (N_a) being the number of electrons (sites)], the TL-liquid theory holds in the small-J region below $J_c/t=2.5-3.5$, depending on n. A phase separation takes place in the larger J/t; there is a region in which the superconducting correlation is dominant, between the phase separation and the supersymmetric case.

Meanwhile, as for physical quantities such as the momentum distribution function or spin- and charge-correlation functions, only the long-range behaviors were clarified in the above analytic methods; the global features were calculated numerically. In the limit of $J/t\rightarrow 0$, identical with the large-U limit of the Hubbard model, the correlation functions were obtained by taking advantage of the spin-charge separation in the ground state.[12] For the other values of J/t, Assaad and Würtz[13] and Imada[14] have carried out quantum Monte Carlo simulations. Pruschke and Shiba[15] studied the superconducting correlation functions by the exact diagonalization. All these results are consistent with the correlation exponents obtained by the analytic methods.

Although the ground-state properties in the 1D t-J model have been clarified quite well, it is still important to examine variational wave functions, for the explicit form of the wave function will make the complicated physics easy to grasp. So far, various kinds of variational states have been proposed for strongly correlated systems.[16–23] The Gutzwiller wave function[24] (GWF) was studied numerically[16,17] and analytically.[18,19] These studies concluded that the GWF is excellent for the one-dimensional Heisenberg model, but is unsatisfactory, even qualitatively, in describing the properties of the strong-coupling Hubbard model or of the small-J region of the t-J model. For example, the GWF does not reproduce the $2k_F$ peak in the spin-correlation function; in the momentum distribution, it has a strange enhancement for $k>k_F$. The main reason is that the density correlation is not sufficiently introduced in the GWF, although the spin correlation is well incorporated. These unsatisfactory features are partly remedied by introducing Jastrow-type intersite correlation factors.[20,22,23]

In a preceding paper,[22] we showed that the behaviors obtained by the exact diagonalization for $J/t=2$ are described extremely well by the GWF and that the wave function is improved for other values of J/t by introducing intersite correlation factors called Jastrow factors.

In this paper we give detailed descriptions of these issues first. Then we compare the above Fermi-liquid-type correla-

tion factors with a TL-liquid-type one introduced by Hellberg and Mele,[23] which has long-range Jastrow factors and thus has nontrivial correlation exponents. It is found that the long-range behavior of the Jastrow factor is essential for the nontrivial exponent or non-Fermi-liquid behavior. On the other hand, the variational energy and the global features of the correlation functions are determined mainly by the short-range behavior of the Jastrow factor. We also show that quantities like χ_c, χ_s and the magnetization curve obtained by the above wave functions are not only qualitatively but quantitatively consistent with the exact results. This aspect is in sharp contrast with the so-called Brinkman-Rice transition.

The outline of this paper is as follows: We give detailed descriptions of and complementary discussions to the preceding letter,[22] namely, the diagonalization results, the properties of the GWF for the supersymmetric case, and the Fermi-liquid-type Jastrow wave functions in Secs. II–IV, respectively. In Sec. V an essentially long-range correlation (TL-liquid-type) factor is examined and compared with the Fermi-liquid-type correlation factors. In Sec. VI, χ_c, χ_s and magnetization curve are investigated. Section VII is assigned to a summary. In Appendixes A and B, an analytical approach to the GWF used in Sec. III and the behavior of χ_c and χ_s in the Gutzwiller approximation compared in Sec. VI are summarized, respectively. A part of the results in this paper has been published also in a review before.[25]

II. GROUND-STATE PROPERTIES OBTAINED IN SMALL CLUSTERS

We study the one-dimensional (1D) t-J model defined as

$$\mathscr{H} = \mathscr{H}_t + \mathscr{H}_J, \tag{2.1}$$

$$\mathscr{H}_t = -t \sum_{j\sigma} \left(c^{\dagger}_{j\sigma} c_{j+1\sigma} + \text{H.c.} \right), \tag{2.1a}$$

$$\mathscr{H}_J = J \sum_j \left(\mathbf{S}_j \cdot \mathbf{S}_{j+1} - \frac{1}{4} n_j n_{j+1} \right), \tag{2.1b}$$

in the subspace with no double occupancy with t, $J \geqslant 0$. Spin operators vanish when they are applied to empty sites. Henceforth we take t as the unit of energy.

We use the Lanczos method and the conjugate gradient method[26] to obtain the ground-state wave function in small clusters. We calculate the momentum distribution function

$$n(k) = \langle c^{\dagger}_{k\sigma} c_{k\sigma} \rangle \tag{2.2}$$

and spin- and charge-correlation functions

$$S(k) = \frac{1}{N_a} \sum_{j,l} 4 \langle S^z_j S^z_l \rangle e^{ik(r_j - r_l)},$$

$$N(k) = \frac{1}{N_a} \sum_{j,l} \{ \langle n_j n_l \rangle - \langle n_j \rangle \langle n_l \rangle \} e^{ik(r_j - r_l)}, \tag{2.3}$$

obtained exactly for various values of J. The data of these quantities were shown in the previous paper[22] for $n = 0.5$.

The global features of the correlation functions for small values of J resemble the results in the large-U Hubbard model.[12] As J increases, they lose this behavior, and near the supersymmetric case ($J/t = 2$), the system behaves similarly to the noninteracting case. This corresponds to the fact that the exponent K_ρ becomes 1 (free-electron value) near $J/t = 2$ ($J/t \sim 2.3$ for $n = 0.5$).[11] $N(k)$ and $S(k)$ become almost flat in the region $k > 2k_F$, which is the same behavior as in the noninteracting case. However, note that these global features of correlation functions are nontrivial even if $K_\rho = 1$, since this exponent only guarantees that the long-range behavior of correlation functions is the same as in the noninteracting case. Actually, the absolute value in the flat region is quite different from the noninteracting value. For the case of 8 electrons in 16 sites, we get

$$N(k > 2k_F) = 0.312 - 0.319,$$

$$S(k > 2k_F) = 0.698, \tag{2.4}$$

while in the noninteracting case $N(k > 2k_F) = S(k > 2k_F) = n = 0.5$. The sum of these two values is, however,

$$N(k > 2k_F) + S(k > 2k_F) = 1.001 - 1.009, \tag{2.5}$$

and this is surprisingly close to the noninteracting value ($2n = 1$).

Since the summation of them is rewritten as

$$\frac{1}{N_a} \sum_{j,l} \{ 2 \langle n_{j\uparrow} n_{l\uparrow} \rangle + 2 \langle n_{j\downarrow} n_{l\downarrow} \rangle - \langle n_j \rangle \langle n_l \rangle \} e^{ik(r_j - r_l)}$$

$$= \frac{4}{N_a} \sum_{j,l} \{ \langle n_{j\uparrow} n_{l\uparrow} \rangle - \langle n_{j\uparrow} \rangle \langle n_{l\uparrow} \rangle \} e^{ik(r_j - r_l)}, \tag{2.6}$$

the sum of $N(k)$ and $S(k)$ represents the density correlation between the same species of spin. The coincidence of this quantity to the noninteracting value shows that each spin behaves freely. This is because the Gutzwiller wave function (GWF) is an extremely good variational state for $J/t = 2$ as shown previously.[22] The Gutzwiller projection only affects the correlation between the different species of spins, such as $\langle n_{j\uparrow} n_{l\downarrow} \rangle$, so that the density correlation between the same species of spins resembles the free case.

Next we estimate the ground-state energy. The ground state is always singlet and nondegenerate, if we choose periodic (antiperiodic) boundary conditions for $N/2 =$ odd (even), respectively.[12,11] Under these boundary conditions, the energy converges smoothly to the thermodynamic limit. For $n = 0.5$ we calculate the ground-state energies in 4-, 8-, 12-, and 16-site clusters and fit the results to the formula

$$E/N_a = \epsilon_\infty + C_1/N_a^2 + C_2/N_a^4 + C_3/N_a^6. \tag{2.7}$$

The fitted values of ϵ_∞ are shown in Table I. In the region $J/t \geqslant 3.4$, the energies cannot be fitted to this formula because the system phase separates in this region and the size dependence is different from Eq. (2.7). To check the convergence for $J/t < 3.4$, we calculate another series of singlet energies by using different boundary conditions, i.e., antiperiodic ones for $N/2 =$ odd and vice versa.[27] Fitting of the data to the same formula, Eq. (2.7), gives another estimate of the ground-state energy (ϵ'_∞), which are also shown in Table I. The difference between ϵ_∞ and ϵ'_∞ is very small ($\Delta\epsilon_\infty < 10^{-6} t$),[28] which ensures the reliability of the esti-

TABLE I. Ground-state energies of the 1D t-J model for the quarter-filled case ($n=1/2$). They are extrapolated to the thermodynamic limit using the formula (2.7). ϵ_∞ and ϵ'_∞ are obtained from the two sets of boundary conditions (see the text). The unit of the energy is t.

J/t	ϵ_∞	ϵ'_∞
0.0	−0.6366197	−0.6366198
0.2	−0.6578750	−0.6575043
0.4	−0.6804029	−0.6806269
0.6	−0.7041767	−0.7041768
0.8	−0.7291701	−0.7291701
1.0	−0.7553587	−0.7553586
1.2	−0.7827211	−0.7827209
1.4	−0.8112399	−0.8112396
1.6	−0.8409031	−0.8409028
1.8	−0.8717049	−0.8717046
2.0	−0.9036477	−0.9036477
2.2	−0.9367449	−0.9367452
2.4	−0.9710250	−0.9710259
2.6	−1.0065398	−1.0065415
2.8	−1.0433801	−1.0433827
3.0	−1.0817130	−1.0817179
3.2	−1.1219079	−1.1219533

mate. For $n=3/4$, we estimate similarly the ground-state energy by using 8- and 16-site clusters with 6 and 12 electrons, respectively. The obtained ϵ_∞ is shown in Table II. Because in this case we fit the data with two parameters ϵ_∞ and C_1, the error is larger than that in the quarter-filled case. We will use ϵ_∞ later to compare with the variational energies.

III. COMPARISON WITH THE GWF NEAR THE SUPERSYMMETRIC CASE

In this section we compare the ground-state properties for $J/t=2$ with the Gutzwiller wave function (GWF). The GWF is defined as

$$P_d\Phi_F=\prod_j (1-n_{j\uparrow}n_{j\downarrow})\Phi_F, \tag{3.1}$$

TABLE II. Ground-state energies of the 1D t-J model for $n=3/4$ similarly obtained as in the quarter-filled case in Table I.

J/t	ϵ_∞	ϵ'_∞
0.0	−0.4501050	−0.4502187
0.2	−0.5216656	−0.5219004
0.4	−0.5943201	−0.5944475
0.6	−0.6678961	−0.6680324
0.8	−0.7422736	−0.7424195
1.0	−0.8173650	−0.8175213
1.2	−0.8931052	−0.8932726
1.4	−0.9694457	−0.9696252
1.6	−1.0463508	−1.0465437
1.8	−1.1237962	−1.1240038
2.0	−1.2017671	−1.2019909
2.2	−1.2802580	−1.2805002
2.4	−1.3592732	−1.3595368
2.6	−1.4388286	−1.4391186
2.8	−1.5189551	−1.5192801
3.0	−1.5997064	−1.6000835
3.2	−1.6811763	−1.6816414
3.4	−1.7635421	−1.7641837

where Φ_F is a simple Fermi sea. In the 1D case, the analytic expression for the physical quantities were developed.[18,19]

First let us compare the variational energy. The expectation value of the kinetic energy is calculated as

$$E_t=\frac{\langle\mathscr{H}_t\rangle}{N_a}=-\frac{2t}{2\pi}\sum_\sigma\int_{-\pi}^{\pi}dk\cos k\langle c^\dagger_{k\sigma}c_{k\sigma}\rangle, \tag{3.2}$$

where $\langle\cdots\rangle$ indicates the expectation value in the GWF. The analytic expression for $\langle c^\dagger_{k\sigma}c_{k\sigma}\rangle$ has been given by an infinite summation.[18] The detailed calculation is summarized in Appendix A. Here we show that the exchange energy can be obtained in a compact form.[19] From the expression of $S(k)$ and $N(k)$ (Appendix A), we get

$$\langle 4S^z_iS^z_{i+1}\rangle=-\frac{1}{\pi}\{\mathrm{Si}(\pi)-\mathrm{Si}((1-n)\pi)\},$$

$$\langle n_in_{i+1}\rangle=n^2+\frac{1}{2\pi^2}(\cos 2n\pi-1)+\frac{1}{\pi}\left(\frac{\sin n\pi}{\pi}+(1-n)\cos n\pi\right)\{\mathrm{Si}(\pi)-\mathrm{Si}((1-n)\pi)\}, \tag{3.3}$$

with $n=N/N_a$ being the electron density. Using the fact that the GWF is a singlet,[29] we obtain, analytically,

$$E_J=\frac{\langle\mathscr{H}_J\rangle}{N_a}=-\frac{J}{4\pi}\left\{\left\{3+\frac{\sin n\pi}{\pi}+(1-n)\cos n\pi\right\}\{\mathrm{Si}(\pi)-\mathrm{Si}((1-n)\pi)\}+\pi n^2+\frac{1}{2\pi}(\cos 2n\pi-1)\right\}. \tag{3.4}$$

It was shown[22] that the total energies of the GWF and that of the Bethe ansatz (BA) at $J/t=2$ are indistinguishable for any value of n. In the low-density limit, the total energy of the GWF at $J/t=2$ is

$$E(\mathrm{GWF})/t=-2n+\frac{\pi^2}{12}n^3+O(n^4), \tag{3.5}$$

which coincides with the BA results up to the order of n^3. The detailed calculation for Eq. (3.5) is also given in Appendix A. This is consistent with the fact that the critical exponent K_ρ approaches 1 for $n\to 0$. This Fermi-liquid state is nothing but the GWF.

The GWF and small cluster calculation give almost the same results for $n(k)$ except for the singularity at k_F. The slight difference between the GWF and exact ground state is the behavior around k_F, which originates from the TL-liquid nature. It is remarkable that the ground state of the t-J model has an enhancement of $n(k)$ in the vicinity of π, which was considered before as a pathological behavior of the GWF.[17] It can be shown that this enhancement originates from the correlated electron motion

$$\langle c^\dagger_{i\sigma}c_{j\sigma}(1-n_{i-\sigma})(1-n_{j-\sigma})\rangle_0, \tag{3.6}$$

where $\langle\cdots\rangle_0$ represents the expectation value in the free Fermi sea Φ_F without the Gutzwiller projection. After a straightforward calculation, Eq. (3.6) becomes

$$P_{ij\sigma}(1-n_{-\sigma}+n^2_{-\sigma}+\delta_{ij}n_{-\sigma}-P_{ij-\sigma}P_{ji-\sigma}) \tag{3.7}$$

and its Fourier transform is

$$n^0_\sigma(k)-2n_{-\sigma}n^0_\sigma(k)+f_2(k). \tag{3.8}$$

Here $P_{ij\sigma}$ is the Fourier transform of $n^0_\sigma(k)=\theta(k_F-|k|)$ and f_2 is given in Appendix A as one of the lowest-order terms in the analytic calculation. The enhancement of $n(k)$ in the region of $k>k_F$ is roughly reproduced from this simple lowest order, Eq. (3.6).

IV. FERMI-LIQUID-TYPE JASTROW FUNCTIONS

In this section we study the Fermi-liquid-type wave functions to describe the t-J model away from $J/t=2$, keeping the application to higher dimensions in mind. In many-body problems Jastrow-type wave functions with two-body correlation factors are often used. First, notice that the trial state becomes nonsinglet if the Jastrow correlation is spin dependent.[30] Therefore we study here only the spin-independent charge density correlation[31]

$$\Psi=\prod_{jl}\prod_{\sigma\sigma'}\{1-[1-\eta(r_{jl})]n_{j\sigma}n_{l\sigma'}\}\Phi_F, \tag{4.1}$$

where $r_{jl}=|r_j-r_l|$. For $\eta(r)$ simple forms are desirable, satisfying the condition of the t-J model: $\eta(0)=0$. This condition is to project out the double occupancies. In this section we consider two cases in addition to the GWF:

$$\eta(r)=\begin{cases}\dfrac{2}{\pi}\arctan\dfrac{r}{\zeta} & (\mathrm{RJWF}), \quad (4.2a)\\ 1 & (\mathrm{GWF}), \quad (4.2b)\\ 1+\dfrac{\alpha}{r^\beta} & (\mathrm{AJWF}), \quad (4.2c)\end{cases}$$

where $r\neq 0$ and ζ, α, and β are positive variational parameters. The typical forms of $\eta(r)$ are shown in Fig. 1. In these functions, $\eta(\infty)=1$ holds and the value of $\eta(1)/\eta(\infty)$ is finite for every parameter set. This point is essentially different from the function with a long-range Jastrow factor discussed in the next section.

We evaluate the expectation values by the variational Monte Carlo (VMC) method.[16,17] This method gives virtually *exact* expectation values for given trial functions. In the VMC calculations in this work, we use systems with electron number $N=4I+2$ (I is an integer) with the periodic boundary condition. Sample numbers ($3\times10^4-2\times10^5$) and sampling intervals (50 Monte Carlo steps at the maximum) are taken so as to reduce statistical fluctuations enough. In this section we use typically 60- and 72-site systems.

A. Repulsive case

The form Eq. (4.2a), which we call the repulsive Jastrow wave function (RJWF) in this paper, includes repulsive correlation. It prefers configurations with electrons mutually apart. In the limit $\zeta\to 0$, it is reduced to the GWF, Eq. (4.2b). This wave function was previously introduced to study the repulsive Hubbard model in strong correlation.[20] In that work it was found that the RJWF lowers the variational energy in the Hubbard model and it reproduces qualitatively the enhancement at $2k_F$ of $S(k)$. Therefore we expect that the RJWF is suitable also for the small-J region of the t-J model.

In Fig. 2, E_t/t and E_J/J in the RJWF are plotted as a function of ζ for $n=0.5$. As ζ increases, electrons keep apart from each other, and thus E_t tends to decrease and E_J in-

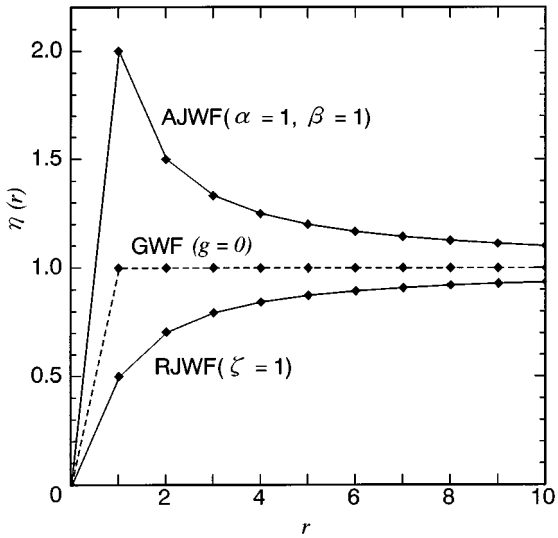

FIG. 1. Correlation factor $\eta(r)$ for three types of Fermi-liquid-type wave functions. Typical values of the parameters are chosen for each case.

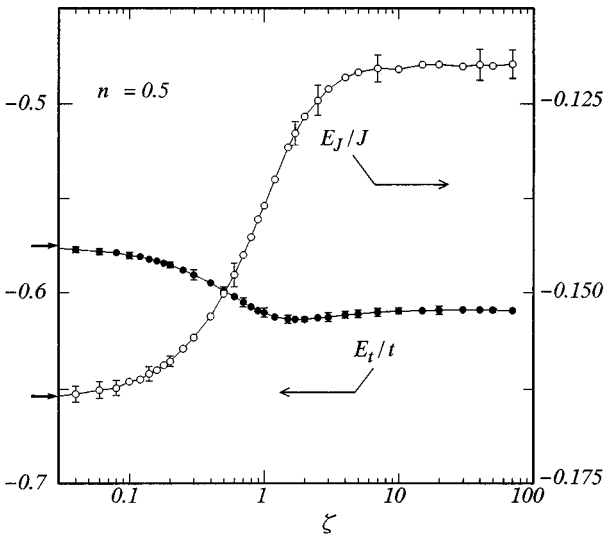

FIG. 2. Expectation values of two energy component $\mathscr{H}_t$ (solid circle) and $\mathscr{H}_J$ (open circle) per site for the RJWF for $n=0.5$. The value of the GWF ($\zeta=0$) is shown by arrows on the vertical axis. We use 3×10^4 samples for a 60-site system.

creases. We show the total energy $E(\zeta)$ for $J/t=1.0$, as an example, in Fig. 3 using the values in Fig. 2. The minimum is situated at $\zeta\sim0.7$; the energy is considerably improved upon the GWF ($\zeta=0$). Similarly we find that the minimum appears at $\zeta\sim1.6$ (for $J/t=0$), 1.2 (0.5), 0.7 (1.0), 0.4 (1.5), and 0 (2.0), respectively. The repulsive interaction represented by the magnitude of ζ becomes weaker with increasing J.

Next, let us consider the critical value J_c below which the RJWF has a lower variational energy than the GWF. In order to estimate J_c, we only have to see the ζ dependence of the variational energy near $\zeta=0$: If the slope of the energy at $\zeta=0$ is positive, the optimal state is $\zeta=0$, which is the GWF. On the other hand, if the slope at $\zeta=0$ is negative, the variational energy has a minimum at a certain value of $\zeta>0$ and the RJWF is more stable than the GWF ($\zeta=0$).

In Fig. 4 variational expectation values E_t/t and E_J/J in the RJWF are shown for $n=0.3$ and small ζ. From this

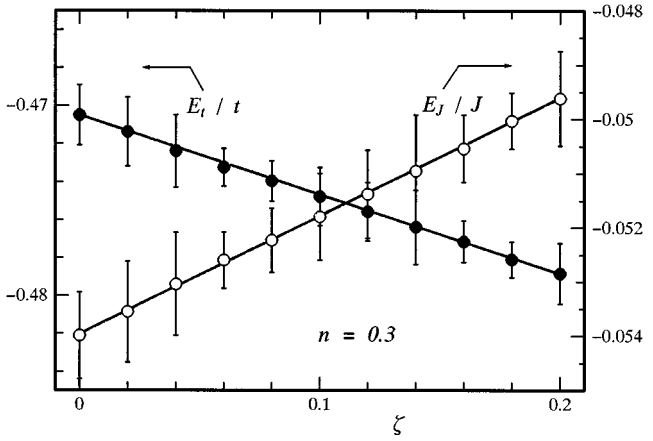

FIG. 4. Expectation values of two energy component $\mathscr{H}_t$ (solid circle) and $\mathscr{H}_J$ (open circle) per site for the RJW and small-ζ region. In this VMC calculation, 10^5 samples are collected for a 72-site system.

figure we read $E_t(\zeta)/t=-0.471-0.0413\zeta$ and $E_J(\zeta)/J=-0.0540+0.0217\zeta$. Since the total variational energy is given by

$$E(\zeta)=E_t(\zeta)+E_J(\zeta), \tag{4.3}$$

the slope of $E(\zeta)$ near $\zeta=0$ is $-0.0413t+0.0217J$. This means that for $J/t<0.0413/0.0217\simeq1.9$ the slope is negative and the RJWF improves the variational energy upon the GWF. In a similar way, we obtain the value of J_c/t also for $n=0.5$, 0.75, and $0.833\ldots$. As n increases, the statistical fluctuation becomes severe and it is not easy to estimate accurate values. However, we find $J_c/t=2.0\pm0.2$ for the above densities. Actually, the value of J_c/t ought to be slightly shifted to a larger value of J/t in the high-density region, as will be seen in the next section. This is consistent with the diagonalization study.[11]

We make a comparison of correlation functions. Figure 5(a) shows $n(k)$, $S(k)$, and $N(k)$ for the optimized wave function at $J/t=0$ and $n=0.5$, together with the result of exact diagonalization. The reproducibility of the global features is not perfectly good. Figure 5(b) shows similar com-

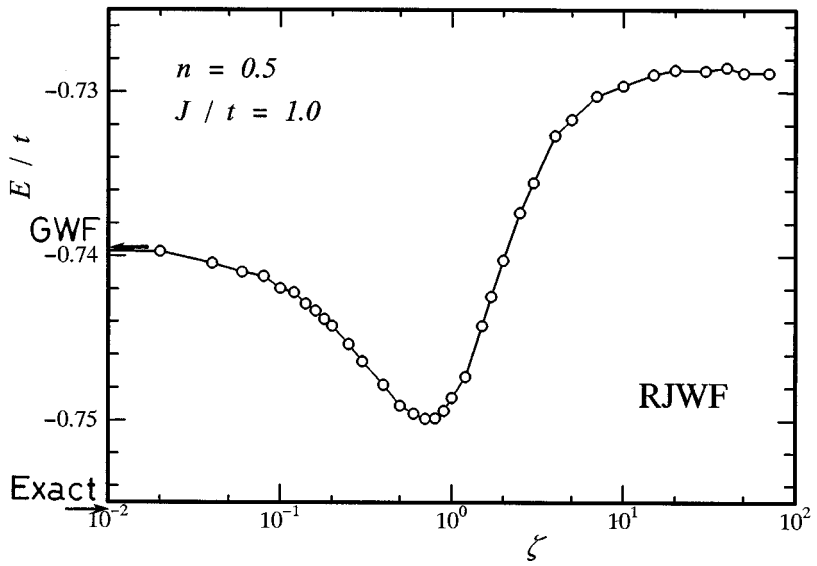

FIG. 3. Energy expectation values for the RJWF at $J/t=1.0$. The arrow on the vertical axis is the value of the GWF and that of the exact diagonalization (extrapolated values for $N_a\to\infty$).

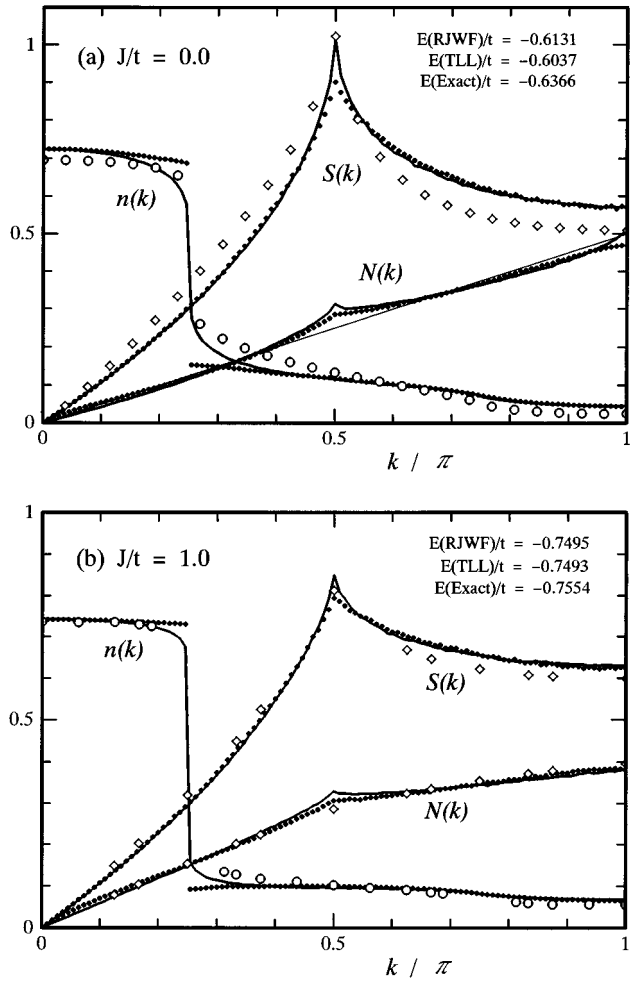

FIG. 5. Comparison of momentum distribution function $n(k)$, spin- and charge-correlation functions $S(k)$ and $N(k)$ among the TL-liquid wave function (bold solid line), the Fermi-liquid-type wave function (dot), and the exact diagonalization [open diamond, open circle, and exceptionally thin solid line for $N(k)$ of $J/t=0$] for (a) $J/t=0$ ($\nu=0.75$ for the TL-liquid state, $\zeta=1.6$ for the RJWF) and (b) $J/t=1$ ($\nu=0.37$, $\zeta=0.7$). For the variational calculations, 10^5 samples are averaged for 220-site systems. The total energy for each case is also given in digits (the last digit for each include the ambiguity due to the statistical fluctuations). For exact diagonalization, 52-site system is used in (a) and up to 16-site systems in (b).

parisons between the variational states and exact diagonalization at $J/t=1$. As J increases, the coincidence becomes better, because the value of J/t is nearer to 2.

The discontinuity q of the momentum distribution $n(k)$ at k_F is plotted in Fig. 6 as a function of n in the optimized variational states. This quantity q is one of the characteristic properties of a Fermi-liquid-type wave function, which is equal to the wave function renormalization factor and related to the inverse of the effective mass m^*/m in the Fermi-liquid theory.

For the supersymmetric case the result of the GWF,[18] $q=\sqrt{1-n}$, is also shown in Fig. 6. In this case q becomes 1 in the limit of $n\to 0$, which is the value of the noninteracting system. In the other limit $n\to 1$, q vanishes. This implies that the Fermi surface vanishes—namely, the effective mass diverges—corresponding to the metal-insulator transition. As

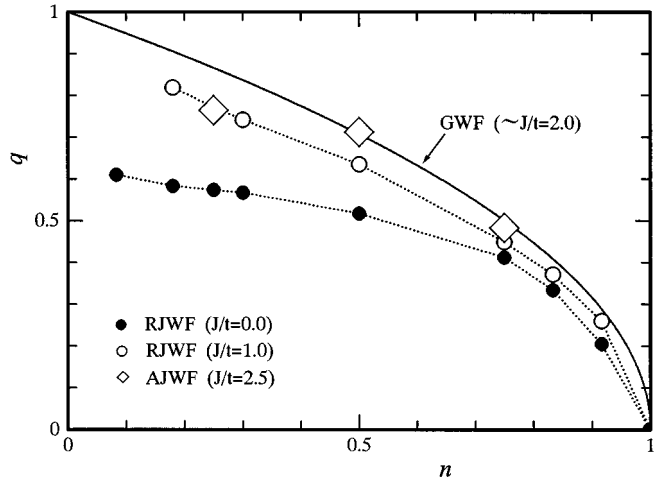

FIG. 6. Discontinuity of momentum distribution $n(k)$ at k_F as a function of n. The optimized Fermi-liquid-type wave function is used for each value of n and J/t. The size of the symbols represent the relative magnitude of possible error. For the cases $n\to 0$ and $J/t\to 0$ and for the AJWF, it is not easy to determine the value accurately owing to the difficulty in optimizing the parameters.

J/t decreases, q becomes small; the correlation affects the whole electron density in this case. Although the result for $J/t=2.5$ includes a relatively large statistical error, it is obvious that q tends to decrease, with increasing J/t from $J/t=2.0$. Thus we conclude that the supersymmetric case is the most weakly interacting; as J/t goes away from it, the correlation effect becomes severer.

B. Attractive case

An attractive Jastrow wave function (AJWF) with the correlation factor Eq. (4.2c) favors local configurations with electrons close to each other. The parameter α adjusts the amplitude of such attractiveness; as α increases, more emphasis is laid upon attractive electron configurations. On the other hand, the other parameter β controls the decaying behavior of $\eta(r)$. With increasing β, the effective attractive range becomes narrower. It is reduced to the GWF when $\alpha\to 0$ or $\beta\to 0$.

For $J/t>2$, it is natural to expect that the attractive correlation between electrons is dominant. In Figs. 7(a) and 7(b) we show the variational expectation values of $\mathscr{H}_t$ and $\mathscr{H}_J$ for the AJWF ($n=0.75$), respectively. E_J becomes lower and E_t becomes higher as α increases, because the amplitude of configurations with electrons located next to one another increases. Note that E_t abruptly approaches to zero and E_J to the energy of the spin system in the region $\alpha>10$ for $\beta=0.625\sim 1$. This is nothing but a sign of the phase transition.

Actually, the snapshots of electron configurations taken along a Monte Carlo (MC) sweep (Fig. 8) show a formation of an electron cluster for $J/t=3.4$, $\alpha=15$, and $\beta=0.75$. Although a small density fluctuation can be seen near the boundary, this edge effect will be irrelevant as $N_a\to\infty$. Second, the minimized energy is quite close to the energy of the Heisenberg chain corrected by electron density. The charge-density correlation function in real space,

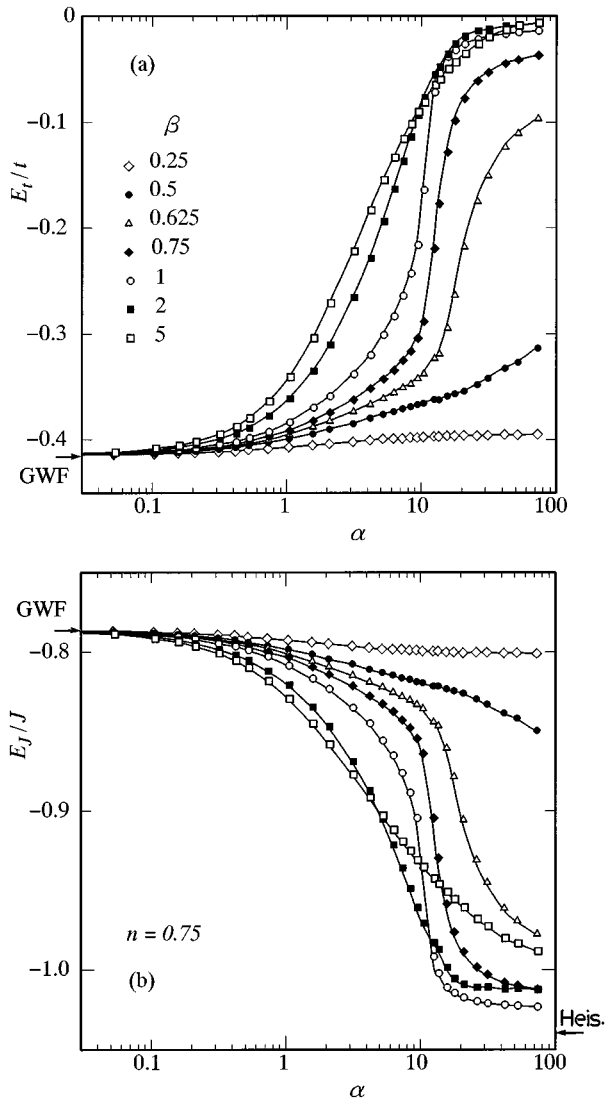

FIG. 7. Variational expectation values of (a) $\mathscr{H}_t$ and (b) $\mathscr{H}_J$ per site for the AJWF. The arrow on the left vertical axis shows the value of the GWF ($\alpha=0$). The arrow on the right axis in (b) shows the value of the Heisenberg chain (Bethe ansatz) multiplied by n. The sample number is 3×10^4 for each point and $N_a=72$.

$$N_r=\frac{1}{N_a}\sum_i\ [\langle n_i n_{i+r}\rangle-n^2], \tag{4.4}$$

for $\alpha>10$, shows that the state is expected as a complete phase-separated state.

Searching a minimum of the variational energy in the α-β plane, we obtain the optimized energy for $J/t>2$. The case of $n=0.5$ has already been shown in Ref. 22. Here we show in Fig. 9 the total energies for $n=0.75$ and $J/t=3.3$, 3.4, and 3.5 as a function of variational parameters. The energy is improved on that of the GWF in every case. The value of α giving the energy minimum becomes large with increase of J/t; this means the enhancement of the attractive correlation.

One can read that the aspects of the minima are quite different among three figures of Figs. 9(a)–9(c). For simplicity, let us consider the case of $\beta=1$ (open circle). In each figure the energy curve of $\beta=1$ has two local minima, that

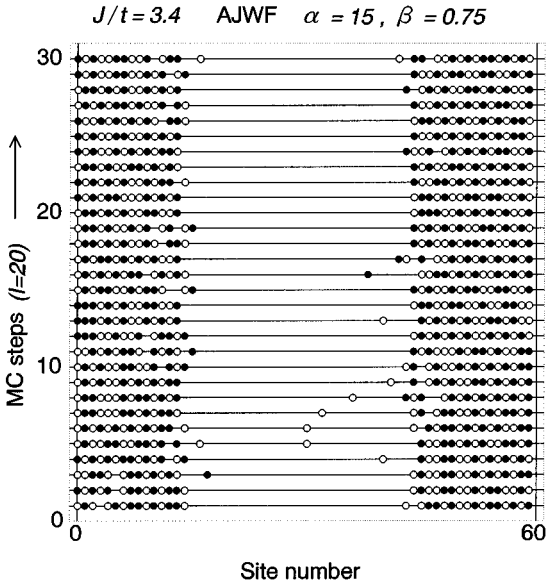

FIG. 8. Snapshots of the electron configurations in the VMC sweep for $N_a=60$, $n=0.5$ at $J/t=3.4$ (separated phase). Each horizontal line represents the one-dimensional system. A solid (open) circle means an up- (down-) spin electron and a null space (horizontal line) an empty site. In the Monte Carlo sweep, the configuration of the system evolves vertically. Before taking these snapshots, 3000 MC steps are discarded for obtaining the statistical equilibrium. The sampling interval is determined ($I=20$ MC steps) so as to make the acceptance ratio per electron larger than the unit.

is, one around $\alpha=1-2$ (minimum H) and one around $\alpha=15$ (minimum S). The latter corresponds to the phase-separated state, as discussed above. In Fig. 9(a) the lowest energy is given by the minimum H and the minimum S has a higher value. In Fig. 9(b) the two minima have comparable values. On the other hand, for $J/t=3.5$ [Fig. 9(c)] the situation is opposite of Fig. 9(a). Thus we find a switching from the state of the minimum H to one of the minimum S around $J/t=3.4$, which represents the phase boundary to the phase separation.

Similarly we obtain $J/t\simeq3.2$ ($n=0.25$) and $J/t\simeq3.3$ ($n=0.5$). These values are in good agreement with the exact-diagonalization result.[11]

V. TOMONAGA-LUTTINGER-LIQUID-TYPE JASTROW FUNCTION

In this section we study the trial state proposed by Hellberg and Mele.[23] For the variational states treated in the previous section, the correlation exponent is always the same as the Fermi liquid ($K_\rho=1$). This is because the Jastrow factor $\eta(r)$ used in Eq. (4.2) approaches 1 rapidly, namely, is short ranged. If the correlation factor $\eta(r)$ is long ranged, the correlation exponent becomes nontrivial, which is consistent with the TL-liquid behavior. Hellberg and Mele[23] showed that a variational state

$$|F(r_{i\uparrow},r_{j\downarrow})|^\nu\Phi_F \tag{5.1}$$

gives nontrivial exponents, where $|F(r_{i\uparrow},r_{j\downarrow})|$ is a Slater determinant of all the electron positions. Actually the correlation exponent is related to the variational parameter ν as[32]

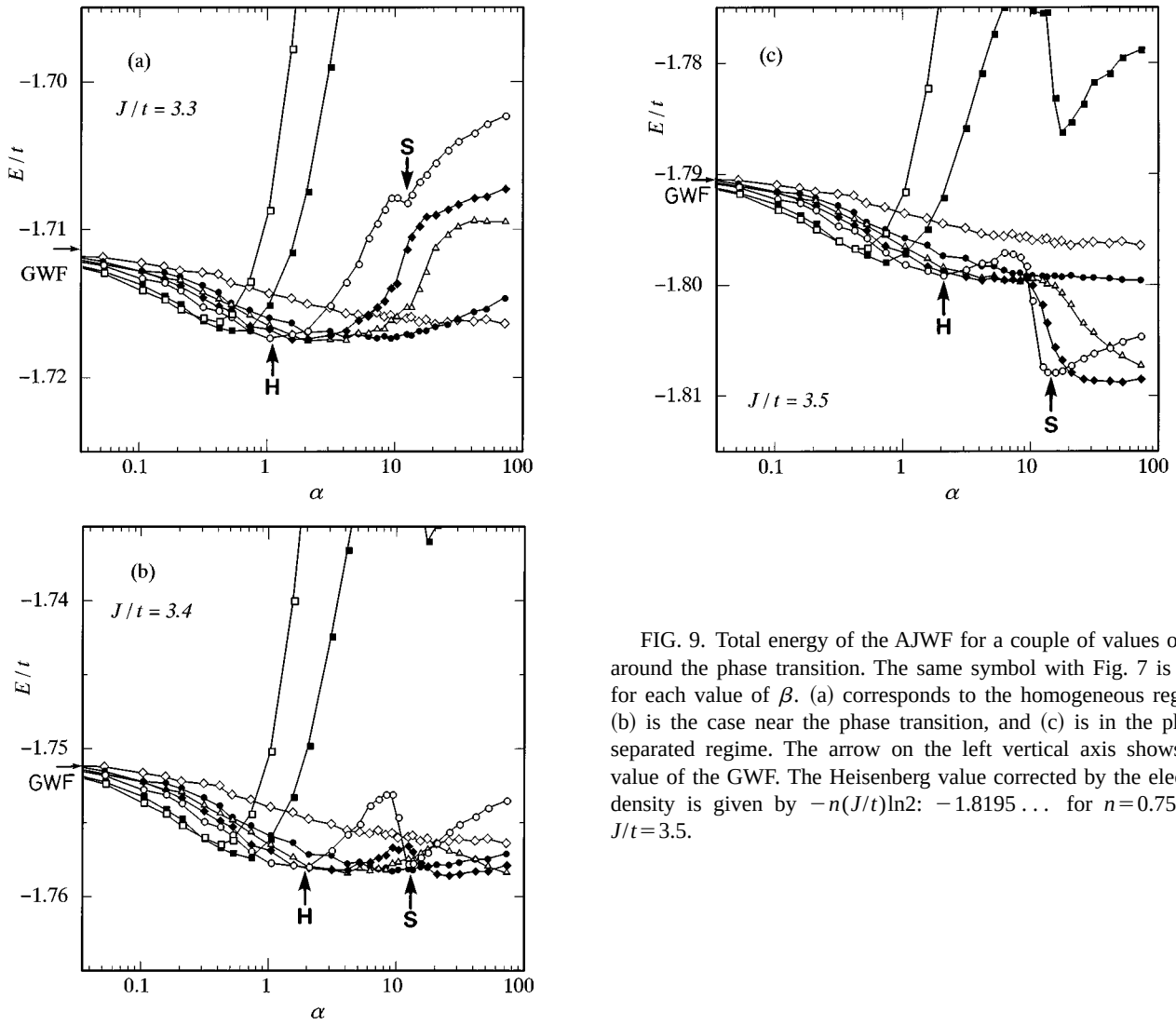

FIG. 9. Total energy of the AJWF for a couple of values of J/t around the phase transition. The same symbol with Fig. 7 is used for each value of β. (a) corresponds to the homogeneous regime, (b) is the case near the phase transition, and (c) is in the phase-separated regime. The arrow on the left vertical axis shows the value of the GWF. The Heisenberg value corrected by the electron density is given by $-n(J/t)\ln 2$: $-1.8195\ldots$ for $n=0.75$ and $J/t=3.5$.

$$K_\rho=\frac{1}{2\nu+1}, \tag{5.2}$$

which was derived using the asymptotic Bethe ansatz and the scaling relations of the TL-liquid theory.

If we rewrite this wave function in the form Eq. (4.1) using the Vandermonde's determinant identity, the corresponding Jastrow correlation can be written as

$$\eta(r)=\left[\frac{N_a}{\pi}\sin\left(\frac{\pi}{N_a}r\right)\right]^\nu. \tag{5.3}$$

When $\nu>0$, this correlation is repulsive and is attractive for $\nu<0$. As we can see from Eq. (5.3), the factor $\eta(r)$ behaves as N_a^ν at the longest distance, $r=N_a/2$. It depends on the system size N_a, and thus it is a very long-ranged Jastrow factor which is different from the conventional Jastrow factor, Eq. (4.2). This long-range behavior stands for the effect of phase shift of two-particle collisions and eventually changes the correlation exponent from the noninteracting value.

The phase diagram obtained with this trial state is given in Fig. 10.[25] Comparing that phase diagram with the one by the exact diagonalization of small clusters,[11] we find that the variational wave function is very good in the vicinity of $J/t=2$ including the correlation exponents, but not so good near $J/t\sim 0$. For example, the optimized variational parameter ν for $J/t=0$ is $\nu=1$ ($\nu=0.75$, $\nu=0.5$) near $n=0$ ($n=1/2$, $n=1$), respectively, while the exact exponent is $K_\rho=1/2$, which corresponds to $\nu=1/2$, regardless of n. One

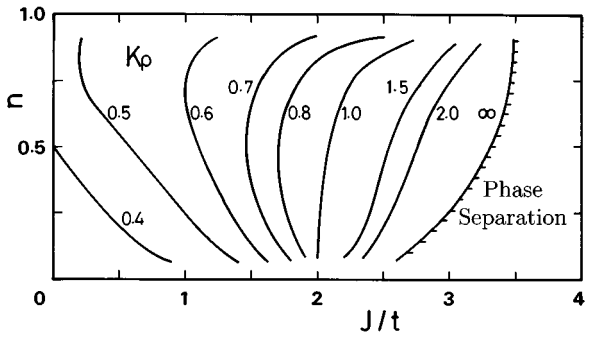

FIG. 10. Phase diagram of the 1D t-J model calculated in the TL-liquid wave function, Eq. (5.1). The curves show the contours of constant correlation exponent K_ρ. The used system has 100 sites.

can see this derivation directly by examining the correlation functions, which are included in Fig. 5. Since the density correlation function $N(k)$ is exactly the same as that of the free spinless fermions at $J/t=0$, there must not be a peak at $2k_F$. However, $N(k)$ calculated with η of Eq. (5.1) has a small peak at $2k_F$ owing to the deviation of the exponent [Fig. 5(a)].

To understand the reason of this deviation, we rewrite the variational state, Eq. (5.1), as[33]

$$|F(r_{i\uparrow},r_{j\downarrow})|^{\nu}\Phi_F=\prod_{i<j}|z_i-z_j|^{\nu}\prod_{i<j}|z_{i\uparrow}-z_{j\uparrow}|\prod_{i<j}|z_{i\downarrow}-z_{j\downarrow}|$$

$$=\prod_{i<j}|z_i-z_j|^{1+\nu}\Big/\prod_{i,j}|z_{i\uparrow}-z_{j\downarrow}|, \tag{5.4}$$

apart from the sign. Here $z_{j\sigma}=\exp(2\pi i r_{j\sigma}/N_a)$ and $\{z_j\}$ represents all the electrons irrespective of their spins. On the other hand, the exact density-correlation function at $J/t=0$ is reproduced by the free spinless fermion, $\Pi_{i<j}|z_i-z_j|$. We can see that it is difficult to reproduce the exact density correlation using the form Eq. (5.4).

In this connection, for the region of $J/t\sim 0$, a better trial function will be obtained as the form, $\Psi=\chi\Phi_{SF}$ on the analogy of the exact eigenfunction in the small-J/t limit,[12] where Φ_{SF} is the wave function of spinless fermion and χ is that for spin degree of freedom.[34]

Figure 5 also shows that the optimized RJWF- and TL-type wave functions give almost identical results. Actually, we find that the two optimized forms of $\eta(r)$ of two variational states are similar in short distance. This suggests that the global features of the correlation functions are determined mainly by the short-range behavior of the Jastrow factor.

Before closing this section we confirm that the long-range part of the correlation factor controls the critical behavior of correlation functions, while the short-range part determines the global features of correlation functions as well as energy. Let us consider the wave functions with four different types of correlation factors, two of which connect the correlation factors of two kinds of variational states, namely,

$$\text{case (1):}\quad \eta(r)=\eta_{\rm TLL}(r)\quad \text{for all } r;$$

$$\text{case (2):}\quad \eta(r)=\begin{cases}\eta_{\rm FL}(r) & \text{for } r<r_c,\\ \eta_{\rm TLL}(r) & \text{for } r\geq r_c;\end{cases}$$

$$\text{case (3):}\quad \eta(r)=\begin{cases}\eta_{\rm TLL}(r) & \text{for } r<r_c,\\ \eta_{\rm FL}(r) & \text{for } r\geq r_c;\end{cases}$$

$$\text{case (4):}\quad \eta(r)=\eta_{\rm FL}(r)\quad \text{for all } r,$$

where $\eta_{\rm TLL}$ denotes $\eta(r)$ of Eq. (5.3), $\eta_{\rm FL}$ either that of the RJWF or AJWF, Eq. (4.2), and r_c is a certain value of r which divides $\eta(r)$ into a short-range part and a long-range part. We choose the variational parameters and r_c so that the two parts may be smoothly connected. By using these correlation factors, we perform VMC calculations for the energy, $n(k)$, $S(k)$, and $N(k)$. We fix the system size to $N_a=100$ for $n=0.5$ and take 5×10^4 samples for each case.

TABLE III. Comparison of expectation values for four kinds of correlation factors hybridized (a) between the RJWF, Eq. (4.2) ($\zeta=6.9847$) and Eq. (5.1) ($\nu=0.5$), for the repulsive case, and (b) between the AJWF, Eq. (4.2) ($\alpha=0.6804$, $\beta=0.5481$) and Eq. (5.1) ($\nu=-0.15$), for the attractive case. Digits include some statistical errors.

	E_t/t	E_J/J	$n(k=0)$	$\delta n(k)<k_F$	$\delta n(k)>k_F$
			(a)		
Case (1)	−0.60865	−0.13972	0.73826	−0.02925	−0.02948
Case (2)	−0.60959	−0.12047	0.70705	−0.02665	−0.02811
Case (3)	−0.60880	−0.13955	0.73804	−0.01958	−0.01989
Case (4)	−0.60983	−0.12037	0.70816	−0.02242	−0.02178
			(b)		
Case (1)	−0.55403	−0.17331	0.74876	−0.00589	−0.01103
Case (2)	−0.54695	−0.17619	0.74777	−0.00309	−0.00559
Case (3)	−0.55392	−0.17334	0.74871	−0.00096	−0.00553
Case (4)	−0.54701	−0.17615	0.74745	−0.00090	−0.00279

For the repulsive case we choose $r_c=5$, $\nu=0.5$ (the optimal value for $J/t\sim 0.7$) and $\zeta=6.9847$. In Table III(a) we show expectation values of several physical quantities for the four cases. $\delta n(k)$ in the last two columns indicates the differences of $n(k)$ between the two possible k points adjacent to k_F from inside and outside, respectively. For the bulk quantities like E_t/t, E_J/J, and $n(k=0)$, cases (1) and (3) give similar values, which are different from cases (2) and (4). This implies that the short-range part of the correlation factor is responsible for the bulk properties like energy and magnitude of correlation functions. On the other hand, for $\delta n(k)$ cases (1) and (2) have similar values compared with cases (3) and (4). This indicates that the long-range part controls the critical behavior of correlation functions.

In Table III(b), the result of the same quantities in the attractive regime is summarized. Here we select $r_c=10$ and $\nu=-0.15$ (the optimal value for $J/t\sim 2.5$) and the two parameters are determined by requesting $\eta_{\rm TLL}(1)=\eta_{\rm AJ}(1)$ and $\eta_{\rm TLL}(r_c)=\eta_{\rm AJ}(r_c)$ as $\alpha=0.6804$ and $\beta=0.5481$. The tendency agrees with the repulsive case. These facts explain the similarity of $n(k)$ and the slight energy difference shown in Fig. 5.

VI. STATIC PROPERTIES OF CHARGE AND SPIN

In this section we focus on the behavior of charge susceptibility χ_c and spin susceptibility χ_s. Since the trial states in the half filling are always Mott insulating for the t-J model, we can see the critical behavior variationally and discuss the difference between the present case and the Brinkman-Rice transition (Appendix B).

We calculate χ_c and χ_s from the VMC data for systems with finite sizes from the formulas

$$\chi_c^{-1}=\frac{\partial^2 E}{\partial n^2}=\frac{N_a^2}{4}\{E(N+2,0)+E(N-2,0)-2E(N,0)\} \tag{6.1}$$

and

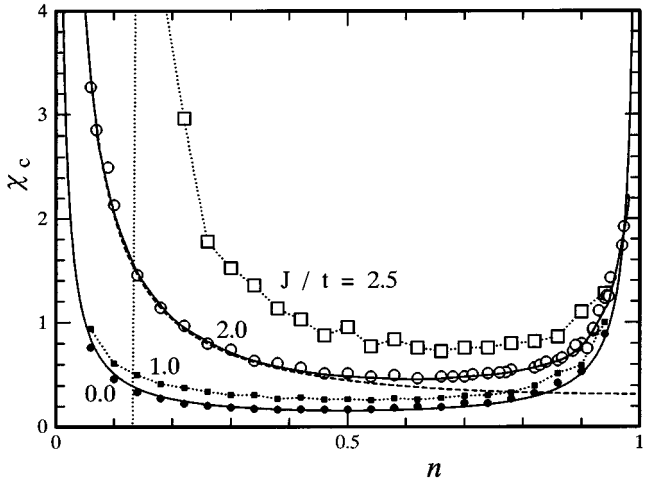

FIG. 11. Charge susceptibility vs n for some values of J/t. Symbols are the results of the optimized TL-liquid state. The solid line for $J/t=0$ and 2 (Ref. 9) represents the exact analytic value. The dashed line is the result for the noninteracting system. The dotted line for $J/t=1.0$ and 2.5 is a guide to the eyes. The sizes of the symbols represent the relative magnitude of possible error. 50–210-site systems are used.

$$\chi_s^{-1}=\frac{\partial^2 E}{\partial m^2}=\frac{N_a^2}{16}\{E(N,8)+E(N,0)-2E(N,4)\}, \tag{6.2}$$

where $E(N,M)$ is total energy per site of N-electron systems with $M=N_\uparrow-N_\downarrow$. Henceforth we take $1/t$ as the unit of χ_c and χ_s. We confirm that the size dependence is mostly negligible for the systems we use: $N_a=100-200$. In contrast to the Hubbard model in the strong-coupling regime, a relatively accurate estimate of χ is possible for the 1D t-J model because of the less statistical fluctuations. In this section, we mainly use the wave function, Eq. (5.3), and GWF. Typically, $5\times10^4-2\times10^5$ independent VMC samples are used for each value of the parameter ν. To search the optimized value of $E(N,M)$ for each N and M, we pick out 61–121 values of ν between -1 and 2.

A. Charge susceptibility

In Fig. 11, χ_c is shown for several values of J/t. Here we observe that with increasing J/t, χ_c becomes large. This is because the enhanced attractive interaction between electrons enlarges the charge compressibility κ $(=\chi_c/n^2)$. In the high-electron-density region $(n\sim1)$, χ_c for every value of J/t is divergent as $n\to1$. This divergence is due to the strong correlation effect, which suppresses charge fluctuation; this is in contrast with the noninteracting case, where $\chi_c^{-1}=\pi\sin(n\pi/2)$ and remains a finite value $1/\pi$ as n approaches 1. For $J/t=0$ and 2, the exact values are known; the spinless fermion result $\chi_c^{-1}=2\pi\sin(n\pi)$ for the former case and the Bethe-ansatz solution for the latter.[4,9] In both cases the exact χ_c diverges as $\chi_c\propto1/\delta$ $(\delta=1-n)$ in the limit of $n\to1$. The variational result is quantitatively similar to the exact one. To see this divergence more closely, we plot chemical potential $\mu=\partial E/\partial n$ vs δ^2 for $J/t=0$ and 2 in Fig. 12. For $J/t\leqslant2$ we can fit μ as $\mu=\mu_0-a\delta^2$ in the vicinity of the half filling, although the linearity is not so clear for $J/t>2$. Since $\chi_c=\partial n/\partial\mu$, the coefficient a is related to the divergence of χ_c as $\chi_c=2a/\delta(\delta\to0)$. From Fig. 12, we determine this coefficient $2a$ for a couple of values of J/t, which are shown in Table IV.

TABLE IV. Coefficient of $1/n$ and $1/\delta$ of charge susceptibility in the limit of $n\to0$ and $\delta\to0$, respectively. For comparison we also show the values of the free-electron system and the supersymmetric t-J model with long-range exchange and transfer, denoted by "Free" and "L.-r. t-J" respectively in the first column.

	$n\to0$		$\delta\to0$	
J/t	Variational	Exact	Variational	Exact
0	0.046	$\frac{1}{2\pi^2}=0.05066$	0.054	$\frac{1}{2\pi^2}=0.05066$
1	0.053	-	0.062	-
2	0.204	$\frac{2}{\pi^2}=0.20264$	0.070	$\frac{16(\ln2)^2}{3\pi^2\zeta(3)}=0.21598$
Free		$\frac{2}{\pi^2}=0.20264$	-	Finite χ_c
L.-r. t-J	Exact	Finite χ_c	Exact	$\frac{2}{\pi^2}=0.20264$

As can be seen in Table IV, the estimation by the variational state is in good agreement with the exact value at $J/t=0$. However, at $J/t=2$, the deviation is quite large. This is probably because the range of linear behavior of μ vs δ^2 is rapidly reduced as J/t increase.[9]

The divergence of χ_c near the Mott transition has been understood from the Bethe ansatz. Using the correlation exponent K_ρ and the charge velocity v_c, χ_c can be written as[5–8]

$$\chi_c=\frac{2}{\pi}\frac{K_\rho}{v_c}.$$

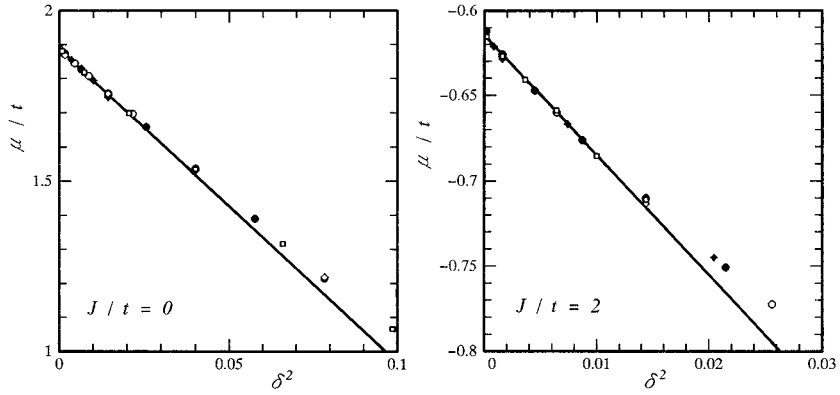

FIG. 12. Chemical potential as a function of δ^2 for $J/t=0$ and 2. Symbols indicate different system sizes, namely, $N_a=200$ (solid diamond), 150 (open circle), 100 (solid circle), 70 (solid square), and 50 (open diamond).

Since v_c vanishes linearly as $\delta \to 0$, $v_c = b\delta$, χ_c diverges as[35,10,14]

$$\frac{2}{\pi}\frac{K_\rho}{b}\frac{1}{\delta}.$$

Since $K_\rho \to 1/2$ as $\delta \to 0$,[11] the coefficient $2a$ is solely related to the coefficient b, which is $2\pi \geq b \geq 3\pi\zeta(3)/16(\ln 2)^2$ for $0 \leq J/t \leq 2$.[11,9] However, for $J/t > 2$, we cannot expand μ as $\mu = \mu_0 - a\delta^2$, but fit μ as $\mu = \mu_0 - a\delta^p$ instead. The leading power p is estimated as $1 < p < 2$, namely, $p = 1.8$ (for $J/t = 2.0$), 1.5 (2.5), and 1.3 (3.0). Although χ_c diverges as $\delta \to 0$ for $J/t \geq 2$, we have not understood the origin of this power. This may be due to the poorness of the trial wave function of Eq. (5.1) or due to an anomalous dependence of v_c as $v_c \sim a\delta^{p-1}$. At any rate, we can consider that this divergence is attributed to the divergence of density of state at the band edge of the spinless fermion.

In low-electron-density area ($n \sim 0$), χ_c again diverges except for the case of $J/t = 2.5$, in which the variational state becomes unstable against phase separation and χ_c becomes negative. One can find that the divergence of χ_c is proportional to $1/n$ by plotting μ as a function of n^2. The coefficients of $1/n$ are shown also in Table IV. Since for $J/t = 2$ the trial wave function (GWF) is exact in the limit $n \to 0$, the exact value is within the range of error. Furthermore, the GWF result and the exact one are extremely close to the noninteracting gas, which means a ''free-electron'' state is realized in the supersymmetric case. Actually, using the variational energy Eq. (3.12), we obtain

$$\chi_c = \frac{2}{\pi^2 n} + O(n^0),$$

which is the same as in the noninteracting case. As n increases, however, the suppression of charge fluctuation in the t-J model prevents the wave function from the free-electron behavior.

For $J/t = 0$ the variational value is a little different from the exact one. This difference corresponds to the deviation of K_ρ in this area, as described in the previous section. The divergence of χ_c is not due to the correlation effect, but simply to the divergence of the density of state at the band edge.

B. Magnetic properties

First, we discuss the spin susceptibility under zero field. Figure 13 shows χ_s for a couple of values of J/t. In sharp contrast to χ_c, χ_s does not diverge as $n \to 1$ for every value of J/t, but remains a finite value close to that of the Heisenberg chain.[36] The divergence of χ_c hardly affects χ_s; this is due to the separation between spin and charge degrees of freedom in the low-energy excitations.

For $J/t = 0$, all the spin configurations are degenerate; hence, χ_s is infinite. This aspect is special in 1D. By introducing J/t, this degeneracy is lifted and the value of χ_s becomes finite except for the low-density limit, which is shown in Fig. 13. In the TL-liquid theory, χ_s can be represented as[5,6,35,7]

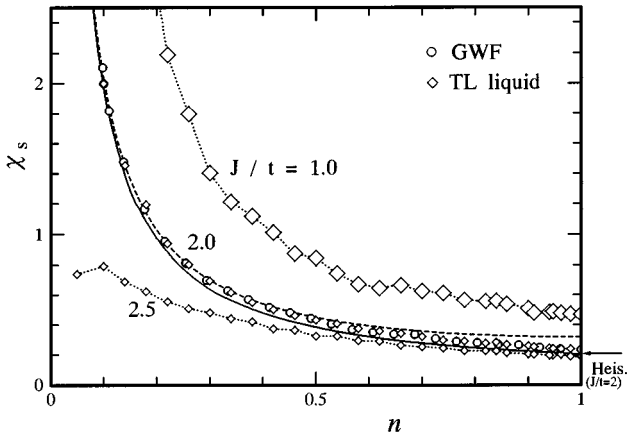

FIG. 13. Spin susceptibility vs n for some values of J/t. The open circle is the result of the GWF for $J/t = 2$ and the open diamonds is the result of the optimized TL-liquid state. The solid line for $J/t = 2$ represents the exact analytical value (Refs. 4,9). The dashed line is the value for the noninteracting system. The dotted line for $J/t = 1.0$ and 2.5 is a guide to the eyes. The arrow on the right vertical axis shows the exact value for the Heisenberg antiferromagnet $2/\pi^2$ for $J/t = 2$ (Ref. 36). The sizes of the symbols represent the relative magnitude of possible error. 50–210-site systems are used.

$$\chi_s = \frac{2}{\pi}\frac{1}{v_s},$$

where v_s is the spin velocity. Basically, v_s is proportional to the exchange coupling J and thus χ_s decreases as J/t increases, which means that the enhanced exchange coupling hinders the response of spins to the magnetic field. For a low-density area ($n \sim 0$), χ_s diverges since $v_s \propto n$, which is due to the divergence of density of states. On the other hand, as $n \to 1$, χ_s approaches that of Heisenberg chain,

$$\chi_s \to \frac{2}{\pi}\frac{1}{v_{\mathrm{SW}}},$$

with s_{SW} being the spin-wave velocity of Heisenberg chain: $v_{\mathrm{SW}} = J\pi/2$.

For the supersymmetric case, we observe that the variational results agree quite well with that of the noninteracting system (Pauli paramagnetism) $\chi_s^{-1} = \pi \sin(n\pi/2)$, especially in the low-density region. Here the idea of the GWF as a ''free-electron'' state is again useful. Like χ_c, however, the two results become a little apart as $n \to 1$. For $J/t = 2.5$ and $n < 0.1$, the decrease of χ_s is due to the phase separation.

Now let us turn to the case under a finite magnetic field $g\mu_B H$, and here we put $g = 2$ and $\mu_B = 1$. Applying an external field along z axis, a Zeeman term

$$\mathscr{H}_{\mathrm{ext}} = -2H\sum_j S_j^z = -N_a H m \tag{6.3}$$

is added to the original Hamiltonian, Eq. (2.1). The total energy per site is written as

$$E = E(m,n) - Hm, \tag{6.4}$$

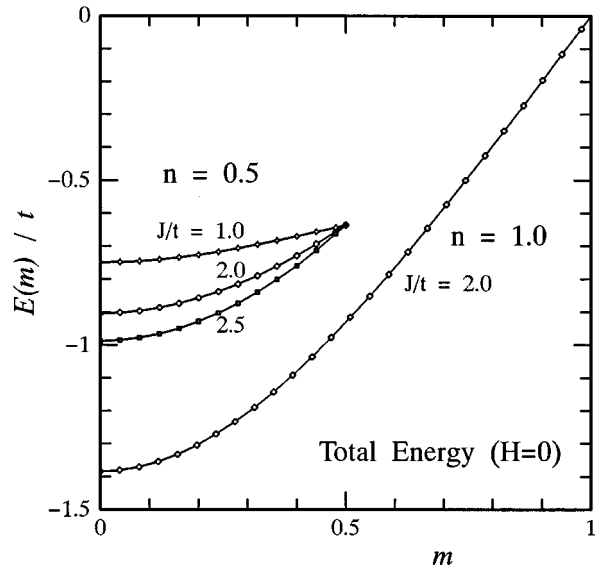

FIG. 14. Total energy under zero field as a function of m calculated with the TL-liquid wave function. For the half filling, where the TL-liquid state is reduced to the GWF, the value in the supersymmetric case is shown for an example. For $n=1.0$ (0.5), a 102- (100-) site system is used. 5×10^4 samples are averaged.

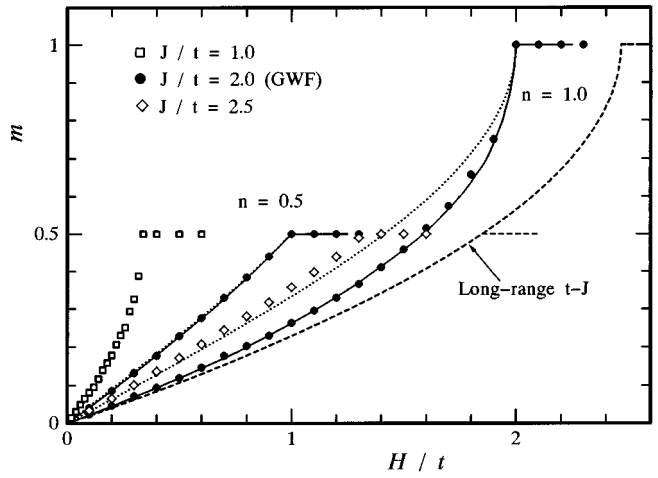

FIG. 15. Comparison of magnetization curves for $n=0.5$ and 1.0. Symbols represent the result of the variational functions. The optimized TL-liquid wave functions are used except for the supersymmetric case, in which the GWF is substituted. The solid line is the Bethe-ansatz result for $J/t=2$ (Refs. 36,38). The dotted line is the result for the noninteracting system. The result for the supersymmetric long-range-t-J model is shown by the dashed line (Refs. 43,44).

where $E(m,n)$ is the total energy per site with electron density n and magnetization m under zero field. In Fig. 14, $E(m,n)$ is shown for $n=0.5$ and 1.0 as a function of m $(0\leqslant m\leqslant n)$. For each case the energy is a monotonically increasing function of m. By minimizing the total energy, Eq. (6.4), we obtain the magnetization curves, which are shown in Fig. 15. The critical field H_s at which spin saturates is determined from the slope of $E(m,n)$ near $m=n$. The value of H_s is 0.34 ($J/t=1.0$), 0.99 (2.0), and 1.32 (2.5) for the quarter filling and 2.000 (2.0) for the half filling.

For the half filling, the data of the GWF are very close to the exact value[36] (Heisenberg antiferromagnet) for all the range of H.[37] In the weak-field limit, m/H is nothing but χ_s; the similarity of the two results is obvious from Fig. 13.

For the quarter filling, m saturates at smaller H as J/t decreases. This is naturally understood since the energy to excite the system to a higher spin state becomes less as J/t decreases. In the supersymmetric case, the GWF is in good agreement with the BA result also for the quarter filling.[38] Furthermore, the noninteracting result agrees well for all the values of H/t.

C. Comparisons and discussion

First, we compare the above result with the Hubbard model. Exact results[39,40,35] show that in the limit $n\to1$, χ_c diverges as $\chi_c=\alpha/\delta$, where α is a numeral factor which depends on U/t.[35] The value of α changes from zero for $U/t=0$ to $1/2\pi^2$ for $U/t=\infty$, which is the same with the t-J model with $J/t=0$. On the other hand, χ_s converges upon a finite value as n approaches 1.[39] In the strong-U limit, the expansion coefficient in t^2/U of χ_s is the same as the t-J model. These features qualitatively agree with the variational results of the present study as well as the exact one for the t-J model.

Meanwhile, Otsuka[41] and Furukawa and Imada[10] investigated the critical behavior of χ_c and χ_s for the Hubbard model on 2D square lattices by using quantum Monte Carlo methods. According to their results, essentially the same properties with the 1D models are observed. Thus one can consider that a universal profile of a kind of Mott transition appears in these results of χ_c and χ_s.

Keeping these in mind, next let us compare with the Brinkman-Rice transition in the Hubbard model. As summarized in Appendix B, χ_s calculated with the Gutzwiller approximation diverges when $U\to U_c$ $(n=1)$ or $n\to1$ $(U\geqslant U_c)$. On the other hand, χ_c remains finite for a finite value of U, even if $U>U_c$, although effective mass m^*/m diverges similarly as χ_s. This indicates that the Brinkman-Rice transition describes a quite different type of metal-insulator transition from those in the 1D and 2D Hubbard models and the 1D t-J model.

Last, we mention the results in the long-range t-J model.[42] In this model, susceptibilities are written as

$$\chi_c^{-1}=\frac{\pi^2}{2}(1-n),\quad \chi_s^{-1}=\frac{\pi^2}{2}(1-m). \tag{6.5}$$

Notice that χ_s does not depend on n and χ_c does not depend on m, since the contributions to the energy of n and m are mutually independent, and that there is no system size dependence, because the size-dependent terms in the energy are exhausted in the linear order. The value of χ_s is constant $(2/\pi^2)$ under zero field irrespective of n, which is the same for the nearest-neighbor Heisenberg model and is close to the variational value (GWF). The divergent behavior of χ_c near the half filling is also similar to the t-J model (see Table IV). On the other hand, a quite different feature appears in the low-electron-density region, where there is no divergence. This difference originates in the band structure of the model; the noninteracting long-range model has linear energy dis-

persion and there is no divergence in the density of state at the band edge. From this we can see that electron correlation affects severely the high-electron-density regime, while in the low-density regime the density of states of the original noninteracting system determines the charge susceptibility.

In Fig. 15 we also plot the magnetization curve of the long-range t-J model:[43,44]

$$m=1-2\sqrt{\frac{1}{4}-\frac{H}{\pi^2 t}}. \tag{6.6}$$

This formula does not depend on n. The critical field H_s for the long-range model is somewhat larger ($\pi^2/4$ for $n=1$ and $3\pi^2/16$ for $n=0.5$) than the value of the ordinary t-J model. And the difference is larger for $n=0.5$. This is probably because the long-range exchange terms tend to disturb the ferromagnetic spin alignment. Especially in the low-density region, where the particle distance is large, the long-range terms play important roles.

VII. SUMMARY AND DISCUSSION

We have pursued the ground-state properties of the one-dimensional t-J model in the light of wave functions, as an extension of the preceding paper.[22] By comparing the variational Monte Carlo results with those of the exact diagonalization, the Bethe ansatz and the Gutzwiller approximation, we have obtained some remarkable aspects as follows.

(1) From diagonalization, exact energy, momentum distribution, and spin and charge correlation functions are obtained, which show the unusual behaviors as J/t increases.

(2) In the supersymmetric case ($J/t=2$) the Gutzwiller wave function is an extremely good state for bulk quantities. In the low-density limit, the GWF becomes exact.

(3) The whole parameter space spanned by electron density n and coupling strength J/t is well described by the repulsive or the attractive Jastrow-type wave functions. The parameter space can be roughly divided into

(a) $J/t<2$ repulsive region (RJWF),

(b) $J/t=2$ freelike region (GWF),

(c) $J/t>2$ attractive region (AJWF).

In region (a), the electron hopping term is dominant. In region (c), dominant is the exchange term, which induces attractive interaction. In the supersymmetric case (b), the two terms are well balanced and a kind of ''noninteracting'' state is realized, especially for the low electron density.

(4) The phase transition from a homogeneous state to a phase-separated state is quantitatively described within the AJWF.

(5) In the Jastrow wave functions, the short-range part of intersite correlation factors are responsible for relatively high-energy processes which determine the bulk properties like energy and magnitude of the correlation functions. On the other hand, a long-range part is mainly concerned in low-energy processes near the Fermi surface, which cause the critical properties characteristic of the Tomonaga-Luttinger liquid.

(6) The Jastrow wave functions reproduces the charge and spin susceptibilities and magnetization curve correctly, in contrast with the Gutzwiller approximation.

Keeping these results in mind, we mention some remaining issues.

In the region of low electron density and $J/t>2$, there exists a spin gap state (without a charge gap).[11,45] We have not found an indication of a spin gap in the trial functions used. On the other hand, Chen and Lee[46] introduced a trial state for a gas of singlet pairs and showed that there is a region where this function is stabler than the TL-liquid wave function, Eq. (5.1).

An interesting extension of the present method is to 2D systems. In 2D we do not know even the ground state—the Fermi liquid or the TL liquid for the metallic regime. Furthermore, magnetically ordered phases can be stabilized, near the half filling.[47] Actually the TL-liquid wave function has been extended to a 2D system by Valenti and Gros.[48] According to their results, the energy lowering by their function is very small (1%) compared with the simple Gutzwiller wave function. Also, the critical exponent at k_F in the momentum distribution is small, assuming that it exists. Since critical properties are in a low-energy scale, it may not be easy to judge the realization of a TL-liquid state in 2D only by the stability in energy.

Recently, the behaviors of the specific-heat coefficient, effective mass, χ_c, χ_s, etc., have been investigated experimentally for the high-T_c superconductors and related Mott insulators,[49] in connection with the metal-insulator transition. The results of these experiments together with the theoretical calculations[41,10] have suggested a reconsideration of the appropriate Hamiltonian, namely, whether the simple t-J model is pertinent to describe various aspects of the high-T_c cuprates.

In these contexts, 2D systems have to be further studied with the variation theory.

ACKNOWLEDGMENTS

The authors are grateful to T. M. Rice, H. Shiba, Y. Kuramoto, D. Vollhardt, W. O. Putikka, M. U. Luchini, S. Sorella, and P.-A. Bares for fruitful discussions. One of the authors (H.Y.) thanks N. Kawakami, W. Metzner, Y. Ono, Th. Pruschke, K. Sano, B. S. Shastry, P. G. J. van Dongen, and F. C. Zhang for useful comments. This work is supported partly by Grant-in-Aids for Scientific Research on Priority Areas, ''Computational Physics as a New Frontier in Condensed Matter Research,'' ''Science of High-T_c Superconductivity,'' and ''Anomalous Metallic States near the Mott Transition,'' given by the Ministry of Education, Science and Culture, Japan.

APPENDIX A: ANALYTICAL APPROACH TO THE GUTZWILLER WAVE FUNCTION

In this appendix, we summarize the analytic expressions for various expectation values in the GWF. They were developed by Metzner and Vollhardt[18] and by Gebhard and Vollhardt[19] for the Hubbard model. In order to apply to the 1D t-J model, we carry out the calculation of $\langle n_i n_j \rangle$ and $\langle S_i^z S_j^z \rangle$.

The momentum distribution for spin σ is obtained by an infinite summation[18]

$$n_\sigma(k)=n_\sigma^0(k)-(1-g)^2 n_{-\sigma} n_\sigma^0(k)+\frac{1}{(1+g)^2}\sum_{m=2}^{\infty}(g^2-1)^m\{1-(1-g^2)n_\sigma^0(k)\}f_{m\sigma}(k), \tag{A1}$$

where g is identical to $\eta(0)$ in our notation [Eq. (4.1)], and thus $g=0$ for the t-J model. $n_\sigma^0(k)$ is the momentum distribution of the noninteracting system given by $n_\sigma^0(k)=\theta(k_F-|k|)$, and $n_\sigma=n/2$. In the 1D case, $f_m(k)$ is given by a polynomial of order $\leqslant m$. According to the notation in Ref. 18, we can summarize as follows:

$$f_m(k)=\begin{cases} n^m R_m(k) \quad (\text{in region I:} \quad 0\leqslant k\leqslant k_F), \\ n^m Q_m(k)+C_{m-1} \quad (\text{in region II:} \quad k_F\leqslant k\leqslant \min(3k_F, 2\pi-3k_F)), \\ C_{m-1} \quad (\text{in region III:} \quad 3k_F\leqslant k\leqslant \pi \quad \text{when} \quad 3k_F<\pi), \\ n^m[Q_m(k)+Q_m(2\pi-k)]+C_{m-1} \quad (\text{in region IV:} \quad 2\pi-3k_F\leqslant k\leqslant \pi \quad \text{when} \quad 2\pi-3k_F<\pi), \end{cases} \tag{A2}$$

where

$$C_{m-1}=(-1)^m\frac{n^m}{2m},$$

$$R_m(k)=\sum_{j=1}^{m}\frac{R_m^{(j)}}{j!}\left(\frac{k}{2\pi n}-\frac{1}{4}\right)^j,$$

$$Q_m(k)=\sum_{j=1}^{m}\frac{Q_m^{(j)}}{j!}\left(\frac{k}{2\pi n}-\frac{3}{4}\right)^j. \tag{A3}$$

The coefficients of these Taylor series are determined via a recursion relation

$$2(m-j+1)R_{m+1}^{(j)}=-(2m-2j+1)R_m^{(j)}-Q_{m+1}^{(j+1)},$$

$$Q_{m+1}^{(j+2)}=2(m-2j)Q_{m+1}^{(j+1)}+2mR_m^{(j)}-4j(m-j+1)(R_m^{(j)}+R_{m+1}^{(j)}),$$

$$R_{m+1}^{(m+1)}=\begin{cases} 0, & m+1=\text{odd}, \\ -2Q_{m+1}^{(m+1)}, & m+1=\text{even}, \end{cases} \tag{A4}$$

with initial values

$$R_1^{(j)}=-\frac{1}{2}\delta_{j,0},$$

$$Q_{m+1}^{(0)}=Q_{m+1}^{(1)}=0.$$

Apparently, the series in Eq. (A1) gives an expansion with respect to n in the low-density region. For $m=2$, we get

$$f_2(k)=\begin{cases} n^2\left(\dfrac{k^2}{4\pi^2 n^2}+\dfrac{5}{16}\right) & \text{in I}, \\ -\dfrac{n^2}{2}\left(\dfrac{k}{2\pi n}-\dfrac{3}{4}\right)^2+\dfrac{n^2}{4} & \text{in II}, \\ \dfrac{n^2}{4} & \text{in III}, \\ -\dfrac{n^2}{2}\left(\dfrac{k}{2\pi n}-\dfrac{3}{4}\right)^2-\dfrac{n^2}{2}\left(\dfrac{2\pi-k}{2\pi n}-\dfrac{3}{4}\right)^2+\dfrac{n^2}{4} & \text{in IV}. \end{cases} \tag{A5}$$

Then the kinetic energy in the dilute limit is

$$E_t=-2t\left(n-\frac{n^2}{2}-\frac{\pi^2}{24}n^3-\frac{n^3}{3}\right)+O(n^4). \tag{A6}$$

Compact analytic expressions for $S(k)$ and $N(k)$ are

$$S(k)=\begin{cases} -\ln\left(1-\dfrac{|k|}{\pi}\right), & 0\leqslant k<2k_F, \\ -\ln(1-n), & 2k_F<k\leqslant\pi \end{cases} \tag{A7}$$

$(2k_F=n\pi)$, and

$$N(k)=\begin{cases} \dfrac{1}{\pi}-\dfrac{|k|}{2\pi}\ln\dfrac{\left(1-n+\dfrac{|k|}{\pi}\right)}{(1-n)} \quad [0\leqslant k<\min(2k_F,2\pi-4k_F)], \\ \dfrac{|k|}{\pi}-\dfrac{|k|}{2\pi}\ln\dfrac{\left(1+n-\dfrac{|k|}{\pi}\right)}{(1-n)}+\ln\left(1+n-\dfrac{|k|}{\pi}\right) \quad [2k_F<k<\min(4k_F,2\pi-4k_F) \\ \text{when } 2k_F<2\pi-4k_F \text{ or } n<2/3], \\ 2-2n+\dfrac{|k|}{2\pi}\ln\dfrac{\left(n-1+\dfrac{|k|}{\pi}\right)}{\left(1-n+\dfrac{|k|}{\pi}\right)} \quad [2\pi-4k_F<k<2k_F \text{ when } 2\pi-4k_F<2k_F \text{ or } 2/3<n<1], \\ 2n+\ln(1-n) \quad [4k_F<k<\pi \text{ when } 4k_F<\pi \text{ or } n<1/2], \\ 2-2n+\dfrac{|k|}{2\pi}\ln\dfrac{\left(n-1+\dfrac{|k|}{\pi}\right)}{\left(1+n-\dfrac{|k|}{\pi}\right)}+\ln\left(1+n-\dfrac{|k|}{\pi}\right) \quad [\max(2k_F,2\pi-4k_F)<k<\pi \text{ when } \pi<4k_F \text{ or } 1/2<n<1]. \end{cases} \tag{A8}$$

Their Fourier transforms give the spin- and charge-correlation functions in real space. Through a straightforward calculation, we get

$$4\langle S_i^zS_{i+r}^z\rangle=\frac{(-1)^r}{\pi r}\{\mathrm{Si}(\pi r)-\mathrm{Si}((1-n)\pi r)\} \tag{A9}$$

and

$$\langle n_in_{i+r}\rangle=n^2+\frac{1}{2\pi^2r^2}(\cos4k_Fr-1)-\frac{(-1)^r}{\pi r}\left\{\frac{\sin n\pi r}{\pi r}+(1-n)\cos n\pi r\right\}\{\mathrm{Si}(\pi r)-\mathrm{Si}((1-n)\pi r)\}, \tag{A10}$$

where r is an integer, $r\geqslant1$. When $r=1$, Eqs. (A9) and (A10) give the exchange energy given in Eq. (3.3). In the low-density limit, we obtain

$$\langle S_i^zS_{i+1}^z\rangle=-\frac{n^2}{8}-\frac{n^3}{12}+O(n^4)$$

and

$$\langle n_in_{i+1}\rangle=\frac{n^2}{2}+\frac{n^3}{3}+O(n^4). \tag{A11}$$

The total energy is

$$E=-2tn+\left(t-\frac{J}{2}\right)n^2+\frac{\pi^2}{12}tn^3+\left(\frac{2}{3}t-\frac{1}{3}J\right)n^3+O(n^4). \tag{A12}$$

At $J/t=2$, we get Eq. (3.5).

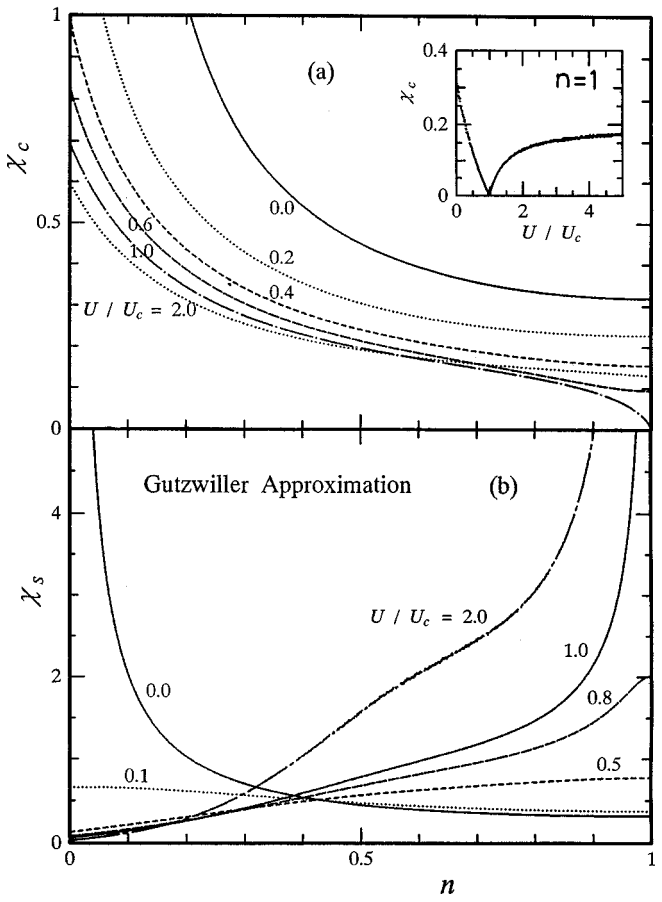

FIG. 16. (a) Charge and (b) spin susceptibilities calculated with Gutzwiller approximation for the Hubbard model as a function of electron density for some values of U/U_c. The inset in (a) represents χ_c vs U/U_c for the half filling. The 1D cosine band is assumed.

APPENDIX B: χ_s AND χ_c AROUND THE BRINKMAN-RICE TRANSITION

Brinkman and Rice discussed the metal-insulator transition for the Hubbard model based on the Gutzwiller approximation (GA).[50] Although it was confirmed by solving the variation problem accurately that this transition does not exist in the realistic (one, two, and three) dimensions,[17,18] the conception of the Brinkman-Rice transition is still widely used. In this appendix we briefly review the behavior of χ_s and χ_c in the GA, especially around the Brinkman-Rice transition for the comparison in Sec. VI.[51]

According to the GA, the states of $n \neq 1$ in the Hubbard model is always metallic and has a Fermi surface with a finite discontinuity q of $n(k)$ at $k=k_F$. On the other hand, in the half filling the GA gives a metallic state for $U<U_c$ and an insulating one for $U>U_c$, where $U_c=8|\varepsilon_0|$ and ε_0 is the energy of the noninteracting system; the Brinkman-Rice transition occurs at $U=U_c$. When U increases from under U_c fixing $n=1$, χ_s as well as effective mass $m^*/m(\propto q^{-1})$ diverges as $1/[1-(U/U_c)^2]$. χ_s and m^*/m remain infinite for $U \geqslant U_c$. Meanwhile, χ_c decreases with increasing U and vanishes at $U=U_c$ and then increases for $U>U_c$. In Fig. 16 we actually plot the numerical GA values of χ_s and χ_c. According to the Fermi-liquid theory, the charge susceptibility is related to m^*/m as

$$\chi_c=\frac{m^*/m}{1+F_0^s}\chi_c^0, \tag{B1}$$

where F_0^s is the usual Landau parameter and χ_c^0 is the value for the noninteracting case. Therefore F_0^s is more divergent than m^*/m at $U=U_c$.

*Electronic address: yoko @cmpt01.phys.tohoku.ac.jp
†Electronic address: ogata @sola.c.u-tokyo.ac.jp

[1] P. W. Anderson, Science **235**, 1196 (1987); F. C. Zhang and T. M. Rice, Phys. Rev. B **37**, 3759 (1988).
[2] E. H. Lieb and F. Y. Wu, Phys. Rev. Lett. **20**, 1445 (1968).
[3] B. Sutherland, Phys. Rev. B **12**, 3795 (1975); P. Schlottmann, *ibid.* **36**, 5177 (1987).
[4] P.-A. Bares and G. Blatter, Phys. Rev. Lett. **64**, 2567 (1990); P.-A. Bares, G. Blatter, and M. Ogata, Phys. Rev. B **44**, 130 (1991).
[5] F. D. M. Haldane, Phys. Rev. Lett. **45**, 1358 (1980); J. Phys. C **14**, 2585 (1981).
[6] H. J. Schulz, Phys. Rev. Lett. **64**, 2381 (1990).
[7] H. Frahm and V. E. Korepin, Phys. Rev. B **42**, 10 553 (1990).
[8] N. Kawakami and S.-K. Yang, Phys. Lett. A **148**, 359 (1990).
[9] N. Kawakami and S.-K. Yang, Phys. Rev. Lett. **65**, 2309 (1990); J. Phys. Condens. Matter **3**, 5983 (1991).
[10] N. Furukawa and M. Imada, J. Phys. Soc. Jpn. **61**, 3331 (1992); **62**, 2557 (1993).
[11] M. Ogata, M. U. Luchini, S. Sorella, and F. F. Assaad, Phys. Rev. Lett. **66**, 2388 (1991).
[12] M. Ogata and H. Shiba, Phys. Rev. B **41**, 2326 (1990); H. Shiba and M. Ogata, Int. J. Mod. Phys. B **5**, 31 (1991).
[13] F. F. Assaad and D. Würtz, Phys. Rev. B **44**, 2681 (1991).
[14] M. Imada, J. Phys. Soc. Jpn. **59**, 4121 (1990); in *Quantum Simulations of Condensed Matter Phenomena*, edited by J. D. Dell and J. E. Gubernatis (World Scientific, Singapore, 1990), p. 127.
[15] T. Pruschke and H. Shiba, Phys. Rev. B **44**, 205 (1991); **46**, 356 (1992).
[16] C. Gros, R. Joynt, and T. M. Rice, Phys. Rev. B **36**, 381 (1987).
[17] H. Yokoyama and H. Shiba, J. Phys. Soc. Jpn. **56**, 1490 (1987).
[18] W. Metzner and D. Vollhardt, Phys. Rev. B **37**, 7382 (1988).
[19] F. Gebhard and D. Vollhardt, Phys. Rev. B **38**, 6911 (1988).
[20] H. Yokoyama and H. Shiba, J. Phys. Soc. Jpn. **59**, 3669 (1990).
[21] C. S. Hellberg and E. J. Mele, Phys. Rev. B **44**, 1360 (1991); Int. J. Mod. Phys. **5**, 1791 (1991).
[22] H. Yokoyama and M. Ogata, Phys. Rev. Lett. **67**, 3610 (1991).
[23] C. S. Hellberg and E. J. Mele, Phys. Rev. Lett. **67**, 2080 (1991).
[24] M. C. Gutzwiller, Phys. Rev. Lett. **10**, 159 (1963); Phys. Rev. **134**, A1726 (1965).
[25] H. Yokoyama, Y. Kuramoto, and M. Ogata, in *Computational*

Physics as a New Frontier in Condensed Matter Research, edited by H. Takayama *et al.* (Physical Society of Japan, Tokyo, 1995), p. 160.

[26] T. Oguchi, H. Nishimori, and Y. Taguchi, J. Phys. Soc. Jpn. **55**, 323 (1986).

[27] In this case, level crossings take place and thus the singlet state does not have the lowest energy in the small-J region. However, we identify the energy level corresponding to the lowest singlet state by following the singlet state as a function of J.

[28] Other combinations of the powers of $1/N_a$ are tried to show that this formula gives the best fitting as expected.

[29] P. W. Anderson, B. S. Shastry, and D. Hristopulos, Phys. Rev. B **40**, 8939 (1989).

[30] If one introduces a spin-dependent correlation factor, keeping the singlet nature, one has to use spin operators isotropically, which means that the Jastrow factor includes off-diagonal elements. This issue is left for future study.

[31] There was an unfortunate typographical error in Eq. (2) of the previous report (Ref. 22). The present Eq. (4.1) is the correct one.

[32] N. Kawakami and P. Horsch, Phys. Rev. Lett. **68**, 3110 (1992); C. S. Hellberg and E. J. Mele, *ibid.* **68**, 3111 (1992).

[33] Suggested by Y. Kuramoto.

[34] M. Ogata, in *Correlation Effects in Low-Dimensional Electron Systems*, edited by A. Okiji and N. Kawakami (Springer-Verlag, Berlin, 1994), p. 121; K. Kobayashi (unpublished).

[35] T. Usuki, N. Kawakami, and A. Okiji, Phys. Lett. A **135**, 476 (1989); N. Kawakami and A. Okiji, in *Strong Correlation and Superconductivity*, edited by H. Fukuyama, S. Maekawa, and A. P. Malozemoff (Springer-Verlag, Berlin, 1989).

[36] R. B. Griffiths, Phys. Rev. **133**, A786 (1964).

[37] For the Hubbard model with finite U/t in the half-filled band, the behavior of the GWF is different. As H approaches H_s, the total energy comes to have two local minima, one of which is at $m=n$. And the global minimum switches from one at $0<m<n$ to the other at $m=n$ abruptly. Thus m has a jump to the full momentum at the critical field. This aspect is common with the Gutzwiller approximation (Ref. 51), but not consistent with the exact result (Ref. 39).

[38] M. Quaisser, A. Schadschneider, and J. Zittartz, J. Phys. A **25**, L1127 (1992).

[39] M. Takahashi, Prog. Theor. Phys. **42**, 1092 (1969).

[40] H. Shiba, Phys. Rev. B **6**, 930 (1972).

[41] H. Otsuka, J. Phys. Soc. Jpn. **59**, 2916 (1990).

[42] Y. Kuramoto and H. Yokoyama, Phys. Rev. Lett. **67**, 1338 (1991).

[43] N. Kawakami, Phys. Rev. B **45**, 7525 (1992); **46**, 1005 (1992).

[44] H. Yokoyama and Y. Kuramoto, J. Phys. Soc. Jpn. **61**, 3046 (1992).

[45] C. S. Hellberg and E. J. Mele, Phys. Rev. B **48**, 646 (1993); Physica B **199 & 200**, 322 (1994).

[46] Y. C. Chen and T. K. Lee, Phys. Rev. B **47**, 11 548 (1993).

[47] H. Yokoyama and H. Shiba, J. Phys. Soc. Jpn. **56**, 3570 (1987); **57**, 2482 (1988); C. Gros, Phys. Rev. B **38**, 931 (1988); Ann. Phys. (N.Y.) **189**, 53 (1989); T. Giamarchi and C. Lhuillier, Phys. Rev. B **43**, 12 943 (1991).

[48] R. Valenti and C. Gros, Phys. Rev. Lett. **68**, 2402 (1992); C. Gros and R. Valenti, Mod. Phys. Lett. B **7**, 119 (1992).

[49] For instance, Y. Tokura *et al.*, Phys. Rev. Lett. **70**, 2126 (1993); K. Kumagai *et al.*, Phys. Rev. B **48**, 7636 (1993); N. E. Phillips *et al.*, in *Progress in Low Temperature Physics*, edited by D. Brewer (Elsevier, Amsterdam, 1990).

[50] W. F. Brinkman and T. M. Rice, Phys. Rev. B **2**, 4302 (1970).

[51] Detailed discussions on the Gutzwiller approximation are given in D. Vollhardt, Rev. Mod. Phys. **56**, 99 (1984).